


Article

A Three-Coil Inductively Power Transfer System with Constant Voltage Output

Ruikun Mai , Youyuan Zhang, Ruimin Dai, Yang Chen and Zhengyou He *

School of Electrical Engineering, Southwest Jiaotong University, Chengdu 610031, China; mairk@swjtu.cn (R.M.); you_yuan_2012@163.com (Y.Z.); ruimindai1992@163.com (R.D.); yang.chen92@foxmail.com (Y.C.)

* Correspondence: hezy@home.swjtu.edu.cn; Tel.: +86-28-8760-2445

Received: 23 January 2018; Accepted: 13 March 2018; Published: 16 March 2018

Abstract: For a traditional 2-coil system outputting constant voltage (CV), the transfer efficiency decreases drastically as transfer distance increases. To solve this problem, this essay proposes a 3-coil system which could achieve CV output and Zero Phase Angle (ZPA) conditions with specific parameter values. This 3-coil system could partly relief transfer efficiency fall at a long transfer distance, without any complicated controls. In order to achieve CV and ZPA condition, this essay devises the parameter values based on the decoupling 3-coil model, and a prototype is designed accordingly to verify these characteristics. With 10 cm transfer distance, output voltage deviation is 5.5% as the load varies from 12 Ω to 200 Ω , proving that the output voltage almost keeps constant with load change. Furthermore, with software simulation, a comparison experiment between the proposed 3-coil system and a Series-Inductor-Capacitor-Inductor (S-LCL) compensated 2-coil system is built to verify the efficiency improvement. The transfer distance change leads to the differentiation of voltage gain for both 2-coil and 3-coil systems. So, the input voltage for both systems and the compensated capacitor in receiver loop of the 3-coil system are manipulated for keeping 60 V output voltage on the 12 Ω load. With distance increasing from 10 cm to 20 cm, transfer efficiency varies from 92.61 to 48.9% for the 2-coil system, and from 92.89 to 84.26% for the 3-coil system, effectively proving the efficiency improvement. The experiment and simulation results prove the effectiveness of the proposed method.

Keywords: relay coil; constant voltage; transfer efficiency; inductive power transfer (IPT)

1. Introduction

Wireless power transfer (WPT) technology can be roughly divided into far-field technology and near-field technology. Within near-field technology, inductive power transfer (IPT) is one of the most explored technology. It utilizes the magnetic field to transfer power [1–4], more convenient and safer than traditional plug-in power transfer system. It has the advantages of flexibility, and avoids the electric shock hazard. For application, IPT technology is largely implemented in biomedical implants, wearable electronics, electric automobiles and rail transport [5–10]. Some applications require constant voltage (CV) for charging, for example, mobile phone [11–14].

Based on a 2-coil resonant tank, achieving CV output is available [15–22], some of which utilize the control method while others adopt elaborate topology. For instance, by implementing two dc-dc converters, where the boost converter after the rectifier circuit for impedance match and the buck converter before the inverter for input voltage conversion, voltage regulation could be performed by manipulating these two dc-dc converters [15]. On the other hand, by using S-LCL topology could also achieving CV [22], which is open loop, has no interconnection between the transmitter and receiver, and easy to control.

However, with 2-coil resonant tank, these power transfer methods fail for high efficiency when transfer distance increases, because the magnetic coupling, which plays an important role in power

transfer, decreases drastically [23]. To relieve the efficiency fall, one method is increasing the working frequency for a high quality factor of the coils so that the conduction loss caused by the coil resistance is reduced [24–26], although it was shown later that this method is not suitable for situations requiring a large amount of delivered power which is inversely proportional to frequency [24]. Besides, the intermediate coil is another way for improving efficiency [27–32], which could create large magnetic coupling with the receiver thus only small current is needed in the primary driving circuit [27]. The working mechanism for the relay coil is that it firstly receives the magnetic field from the transmitter coil and then transfers it to the receiver coil, apparently increases the coupling coefficient resulting a higher efficiency [28]. The optimal coil geometries for a 3-coil IPT system could be found in [23].

These proposals obviously resolve the low transfer efficiency at large coupling distance, but these systems cannot output CV. Some researchers have noticed this problem, and explore how to achieve CV with a relay coil. For example, a 4-coil IPT system could successfully achieve CV when the working frequency is set to a specific value [24,31]. The drawback of this method is that the output voltage involves a lot of variables; a slight change in the system variables may lead to the output voltage deviation.

To reduce the transfer efficiency fall at a larger coupling distance, as well as achieving CV with simple variables, this essay proposes a series-series (SS) compensated 3-coil IPT system. This essay is organized as follows: firstly, analyze the SS compensated 3-coil IPT model, and propose a method to design the parameter values to achieve CV. Besides the 3-coil system, a 2-coil system with S-LCL topology is used to compare the efficiency. Moreover, a prototype based on the 3-coil system is built to verify the feasibility for achieving CV. Finally, with software, the 2-coil system and the 3-coil system are simulated to compare the efficiency as distance changes.

2. Theoretical Analysis

This section mainly focuses on basic principles of the 3-coil system. For better analyses, this part is designed as follows: Section 2.1 introduces the 3-coil IPT system, its Section 2.1.1 will depict the fundamental configuration as well as Kirchhoff's voltage law (KVL) equations to facilitate later analysis. Section 2.1.2 will explain voltage gain and the parameter design process that provides load-independent output voltage. Section 2.1.3 will describe transfer efficiency for the proposed 3-coil system. Section 2.1.4 will devise parameter values. Following Section 2.2 would illustrate the 2-coil parameter design.

2.1. Overview of the Series-Series 3-Coil IPT System

Figure 1 shows the configuration of the proposed series-series compensated 3-coil IPT system. The circuit consists of a constant voltage source E , a full-bridge inverter Q_1 – Q_4 for a square wave generator, a resonant tank including 3 coils: L_1 , L_2 , L_3 and their resonant capacitor C_1 , C_2 , C_3 , a full-bridge diode rectifier D_1 – D_4 and a load R_L . L_1 , L_2 and L_3 represent the transmitter coil, the receiver coil and the relay coil, respectively. M_{ij} ($i, j = 1, 2, 3, i \neq j$) means mutual-inductance between coil i and coil j .

Based on Figure 1, r_s , r_1 , r_2 , r_3 are the parasite and winding resistance of the source, L_1 , L_2 and L_3 , respectively. Relationship between the inverter output voltage U_{in} and the inverter input voltage E is $U_{in} = 2\sqrt{2}E/\pi$. Relationship between the rectifier input voltage U_{out} and the load voltage (U_{RL}) is $U_{out} = 2\sqrt{2}U_{RL}/\pi$.

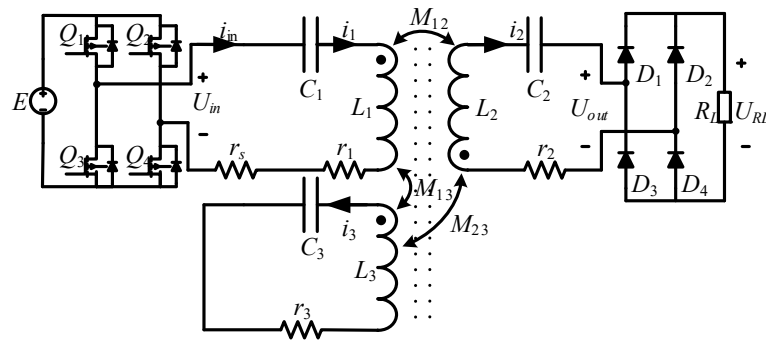


Figure 1. Configuration of the proposed series-series compensated 3-coil IPT (inductive power transfer) system.

2.1.1. Equivalent Circuits and Fundamental Analysis

Figure 2 illustrates the resonant tank of the 3-coil system. Transmitter coil and relay coil are placed on a same plane. The geometric design is shown in Figure 2b: the red loop (Loop 1) is the transmitter coil, the green loop (Loop 2) is the receiver coil, the blue loop (Loop 3) is the relay coil, and the two grey square planes are ferrite bars, one below the transmitter and relay coil, and the other one above the receiver coil.

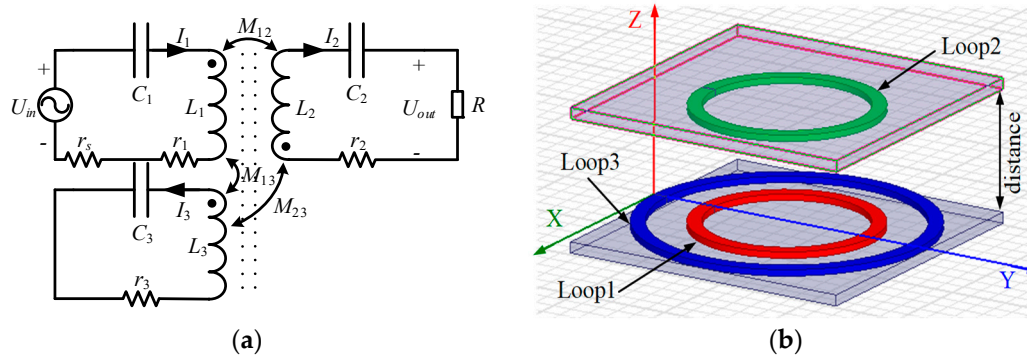


Figure 2. Resonant tank in (a) equivalent circuits model (b) 3D module in Maxwell.

For facilitate analysis, the resonant tank circuit could be described in Equation (1) according to Kirchhoff's law. In Equation (1), X_i ($i = 1, 2, 3$) represents the imaginary component of equivalent impedance for loop i ; I_i represents the current flowing through the loop i ; ω represents the working frequency, R represents the equivalent load, as $R = 8R_L/\pi^2$.

$$\begin{bmatrix} U_{in} \\ 0 \\ 0 \end{bmatrix} = \begin{bmatrix} jX_1 + r_1 + r_s & -j\omega M_{12} & -j\omega M_{13} \\ -j\omega M_{12} & jX_2 + r_2 + R & j\omega M_{23} \\ -j\omega M_{13} & j\omega M_{23} & jX_3 + r_3 \end{bmatrix} \cdot \begin{bmatrix} I_1 \\ I_2 \\ I_3 \end{bmatrix} \quad (1)$$

2.1.2. Voltage Gain and Methodology for CV Mode

This subsection illustrates the voltage gain of the proposed 3-coil system based on Equation (1). The voltage gain G_V is defined as the ratio of the output voltage to the input voltage. For simplicity, X_1 is set to 0, and the winding resistance r_i ($i = 1, 2, 3$) and r_s are neglected, they would be reconsidered in later subsection for transfer efficiency.

G_V could be calculated as Equation (2), with the current derived from Equation (1).

$$G_V = \frac{I_2 R}{U_{in}} = \frac{AR^2 + BR}{CR^2 + D} \quad (2)$$

$$\begin{aligned}
A &= \omega M_{23} M_{13}^3 - X_3 M_{12} M_{13}^3 \\
B &= j(X_3 M_{12} - \omega M_{13} M_{23})(X_3 M_{12}^2 - 2\omega M_{12} M_{13} M_{23} + X_2 M_{13}^2) \\
C &= \omega M_{13}^4 \\
D &= \omega(X_3 M_{12}^2 - 2\omega M_{12} M_{13} M_{23} + X_2 M_{13}^2)^2
\end{aligned} \tag{3}$$

It is shown in Equation (2) that if the D and B equals 0 simultaneously, G_V will not change when the load R varies. Based on this principle, B and D should satisfy Equation (4).

$$\begin{bmatrix} B \\ D \end{bmatrix} = \begin{bmatrix} j(X_3 M_{12} - \omega M_{13} M_{23})(X_3 M_{12}^2 - 2\omega M_{12} M_{13} M_{23} + X_2 M_{13}^2) \\ \omega(X_3 M_{12}^2 - 2\omega M_{12} M_{13} M_{23} + X_2 M_{13}^2)^2 \end{bmatrix} = \begin{bmatrix} 0 \\ 0 \end{bmatrix} \tag{4}$$

By substituting Equation (4) into Equations (3) and (2), Equation (2) could be rewritten as Equation (5).

$$G_V = \frac{A}{C} = \frac{\omega M_{23} - X_3 M_{12}}{\omega M_{13}} \tag{5}$$

It can be seen from the Equation (5) that voltage gain is load-independent now, achieving CV output with Equation (4), X_3 , which is the imaginary component of the equivalent impedance for loop 3, could be rewritten as Equation (6).

$$X_3 = \frac{X_2 M_{13}^2 - 2\omega M_{12} M_{13} M_{23}}{M_{12}^2} \tag{6}$$

By substituting Equation (6) into Equation Equation (5), G_V could be more concise as Equation (7).

$$G_V = \frac{X_2 M_{13} - \omega M_{12} M_{23}}{\omega M_{12} M_{13}} \tag{7}$$

Z_{in} , the equivalent impedance of the resonant tank, is defined as the ratio of input voltage to the input current, shown in Equation (8).

$$Z_{in} = \frac{U_{in}}{I_1} = \alpha + j\beta \tag{8}$$

α , β are the real part and imaginary part of the input impedance of the resonant tank, respectively. To reduce the system's power loss, as well as the capacity requirement for the inverter, the Zero Phase Angle (ZPA) condition should be achieved, β should be set to 0. After some simple mathematical manipulations, X_2 , the imaginary component of the equivalent impedance for loop 2, is derived as Equation (9).

$$X_2 = \frac{2\omega M_{12} M_{23}}{M_{13}} \tag{9}$$

Implementing the new X_2 value, the equivalent impedance Z_{in} is rewritten as Equation (10).

$$Z_{in} = \frac{M_{13}^2}{M_{23}^2} R \tag{10}$$

From Equation (10), it's obvious that the equivalent impedance of the resonant tank is pure resistive, avoiding the reactive power dissipation caused by inductor or capacitor, achieving ZPA condition and decreasing the system's power loss and the capacity requirement for the inverter.

Substituting Equation (9) into Equation (6), X_3 , the imaginary component of the equivalent impedance for loop 3, could be more concise as Equation (11).

$$X_3 = 0 \tag{11}$$

Implementing Equation (9) to Equation (7), G_V can be rewritten as Equation (12). Notice that as distance between transmitter and receiver coils varies, M_{23} and M_{13} also change.

$$G_V = \frac{M_{23}}{M_{13}} \quad (12)$$

To conclude this subsection, if the parameter values satisfy the relationship in Equation (9), (11) as well as $X_1 = 0$, the CV mode could be achieved, as well as ZPA condition. Besides, the G_V could be measured with Equation (12).

2.1.3. Efficiency Analysis

This subsection illustrates the transfer efficiency for the proposed 3-coil system, with the consideration of the winding resistance r_i ($i = 1, 2, 3$) and the source resistance r_s , which are shown in Figure 2.

Figure 2 could be described as the decoupled circuit shown in Figure 3. r_a , r_b , r_c is the reflected impedance from loop 2 to loop 1, from loop 3 to loop 1, from loop 2 to loop 3, respectively, and they are measured in Equation (13).

$$r_a = \operatorname{Re}\left(-j\omega M_{12} \frac{I_2}{I_1}\right), r_b = \operatorname{Re}\left(-j\omega M_{13} \frac{I_3}{I_1}\right), r_c = \operatorname{Re}\left(j\omega M_{23} \frac{I_2}{I_3}\right) \quad (13)$$

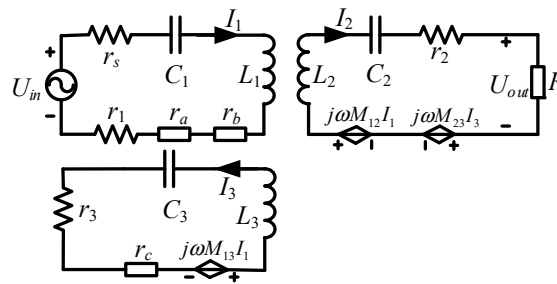


Figure 3. Decoupled circuit of resonant tank for the proposed 3-coil system.

Based on Figure 3, the transfer efficiency could be derived in Equation (14). η_1 , η_2 , η_3 represent the efficiency of loop 1, loop 2 and loop 3, respectively.

$$\eta_1 = \frac{r_a + r_b}{r_a + r_b + r_1 + r_s}, \eta_2 = \frac{R}{R + r_2}, \eta_3 = \frac{r_c}{r_c + r_3} \quad (14)$$

Transfer efficiency for the whole system is shown in Equation (15), which is the multiplication of the three efficiencies above. The components R_{1_23} , R_{3_2} in the numerator are illustrated in Equation (16), and R represents the equivalent load, as $R = 8R_L / \pi^2$.

$$\eta = \eta_1 \eta_2 \eta_3 = \frac{R_{1_23} R_{3_2} R}{(r_1 + r_s + R_{1_23})(r_3 + R_{3_2})(r_2 + R)} \quad (15)$$

$$R_{1_23} = \operatorname{Re}\left(-j\omega M_{12} \frac{I_2}{I_1}\right) + \operatorname{Re}\left(-j\omega M_{13} \frac{I_3}{I_1}\right), R_{3_2} = \operatorname{Re}\left(j\omega M_{23} \frac{I_2}{I_3}\right) \quad (16)$$

2.1.4. Parameter Value Design

This subsection illustrates how to design the parameter values for the proposed 3-coil system. Assuming that the voltage on the dc load R_L is U_{RL} , and input dc voltage is E , the working efficiency is f and $\omega = 2\pi f$. Based on Equation (12), and the relationship between input voltage and output voltage of the inverter and the rectifier, Equation (17) is derived.

$$G_V = \frac{M_{23}}{M_{13}} = \frac{U_{RL}}{E} \quad (17)$$

We set $U_{RL} = 60$ V and $E = 120$ V in the experiment of verifying the CV feasibility, where the distance between receiver and transmitter keeps 10 cm. According to Equation (17), the ratio of M_{23} and M_{13} is fixed as 0.5. Then the software ANSYS Maxwell (Ozen Engineering, Inc., Silicon Valley, Sunnyvale, CA, USA) is involved to design the coil size to meet $M_{23}/M_{13} = 0.5$, so that the three coils' size, turns, relative position, self-inductance L_1, L_2, L_3 as well as the mutual-inductance M_{12} are all determined.

Based on aforementioned requirement $X_1 = 0$, C_1 in the transmitter coil is derived in Equation (18).

$$C_1 = \frac{1}{\omega^2 L_1} \quad (18)$$

Based on Equation (11), C_3 in the relay coil is derived in Equation (20).

$$C_3 = \frac{1}{\omega^2 L_3} \quad (19)$$

Based on Equation (9), C_2 in the receiver coil is shown in Equation (20).

$$C_2 = \frac{M_{13}}{\omega^2 (L_2 M_{13} - 2 M_{12} M_{23})} \quad (20)$$

As the capacitor values satisfy Equations (18)–(20), the proposed 3-coil IPT system could achieve CV as well as ZPA condition.

The transfer distance change would lead to differentiation in mutual-inductance, so that the C_2 should be recalculated according to Equation (20).

2.2. Parameter Design for S-LCL Compensated 2-Coil System

Besides verifying the feasibility for CV of the aforementioned 3-coil system, a comparison experiment is also needed to prove that the 3-coil system has higher efficiency than that of 2-coil system as distance increasing. The methodology for designing parameter values in 2-coil system is illustrated in this Section 2.2.

The S-LCL topology of 2-coil circuit is shown in Figure 4.

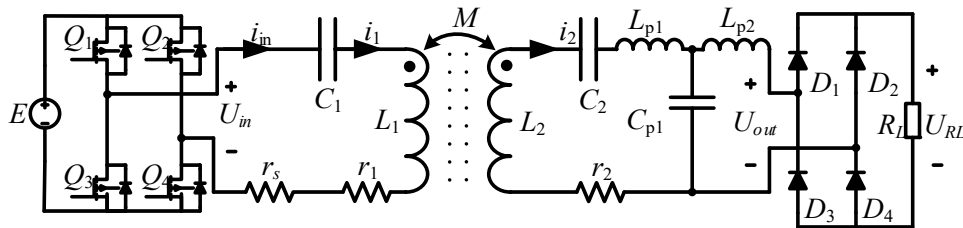


Figure 4. S-LCL compensated 2-coil system from [22].

The voltage gain G_V for the 2-coil system shown in Figure 4 could be derived as Equation (21) based on [22].

$$G_V = \left| \frac{U_{RL}}{E} \right| = \frac{1}{\omega^2 M C_{p1}} \quad (21)$$

For a fair and reasonable efficiency-comparing experiment, we adopted the principle mentioned in reference [33]. For a 2-coil system, the power supply drives the transmitter coil and relay coil in series, so that the same copper volume is used in the coupling mechanism for both 2-coil system and

3-coil system. Besides, G_V for both systems are designed to be the same value, which varies with transfer distance. G_V could be determined with Equation (12).

The capacitor value C_{p1} in Figure 4 could be derived in Equation (22), based on Equation (21).

$$C_{p1} = \frac{1}{\omega^2 M G_V} \quad (22)$$

Based on Equation (22), Inductance values L_{P1} and L_{P2} could be measured with Equation (23).

$$L_{P1} = \frac{1}{\omega^2 C_{p1}}, L_{P2} = L_{P1} \quad (23)$$

Capacitors C_1 and C_2 resonant with L_1 and L_2 , respectively. Their values are shown in Equation (24).

$$C_1 = \frac{1}{\omega^2 L_1}, C_2 = \frac{1}{\omega^2 L_2} \quad (24)$$

If the requirements in Equations (22)–(24) are satisfied, the S-LCL compensated 2-coil system could achieve CV as well as ZPA condition [22].

3. Experimental Analysis

In this experimental part, we firstly build a 3-coil system to test the feasibility for CV. Secondly, with software, we simulate the proposed 3-coil system with the S-LCL 2-coil system, to prove that the former one has higher efficiency as transfer distance changes.

To test the effectiveness of the CV of the 3-coil system, we build an experimental prototype shown in Figure 5a, which includes an oscilloscope (Agilent DSO-X3014T, Santa Clara, CA, USA) to record the experimental output waveforms and a power analyzer (PW6001, HIOKI, Nagano, Japan) to gauge the transfer efficiency between dc source and dc load. The transmitter and receiver coils are wound with Litz wires (0.1×400) as shown in Figure 5b. Parameter values are shown in Table 1.

In Figure 5b, loop 1 is the transmitter coil, which connects inverter comprising 4 MOSFETS (C2M0080120D, Cree, Durham, NC, USA); loop 2 is the receiver coil which connects rectifier including 4 diodes (DSEI2X61-06C, IXYS, Milpitas, CA, USA) and the electronic load (IT8518B, ITECH, NanJing, China), loop 3 is the relay coil to generate an enhanced magnetic flux for the power transfer to receiver [19]. For size, the transmitter coil's outer diameter is 191.5 mm, the same as receiver coil, and the relay coil 300 mm. For relative position, the relay coil and the transmitter coil are remained in the same plane and same centered, the receiver is parallel with the transmitter and same centered; space between relay coil and transmitter is 40 mm, power transfer distance between receiver and transmitter keeps 100 mm in testing the constant voltage output characteristics of the 3-coil system.

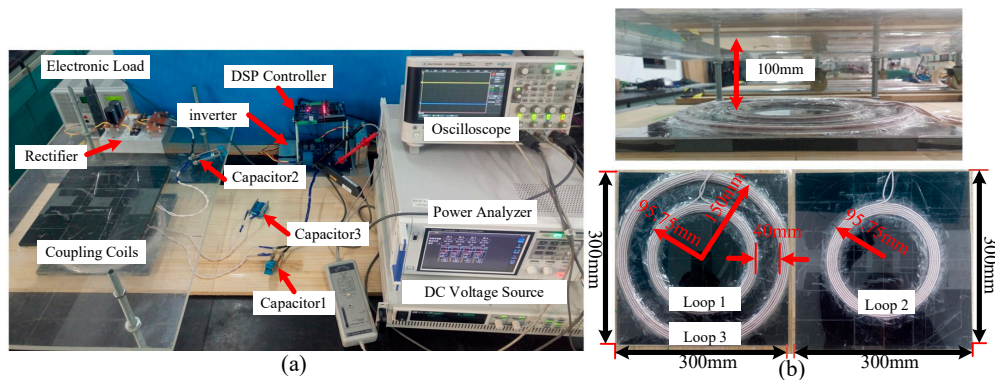
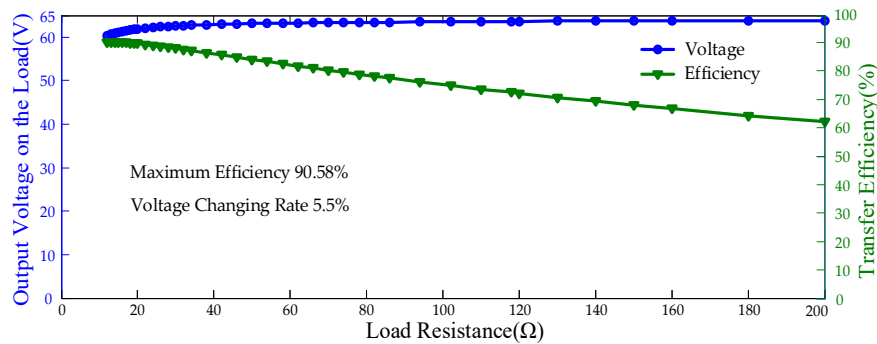


Figure 5. (a) Prototype of the 3-coil system (b) Resonant tank of the 3-coil system.

Table 1. Parameter values for 3-coil system.

Parameter	Value	Parameter	Value
Frequency f /kHz	200	Capacitor C_2 /nF	13.681
Input voltage E /V	120	Capacitor C_3 /nF	6.701
Self-inductance L_1 /uH	53.76	Transfer distance gap/mm	100
Self-inductance L_2 /uH	56.69	Outer radius of Loop 1 R_1 /mm	95.75
Self-inductance L_3 /uH	94.497	Outer radius of Loop 2 R_2 /mm	95.75
Mutual inductance M_{12} /uH	9.5425	Outer radius of Loop 3 R_3 /mm	150
Mutual inductance M_{13} /uH	23.255	Number of turns for Loop 1 N_1	10
Mutual inductance M_{23} /uH	12.675	Number of turns for Loop 2 N_2	10
Capacitor C_1 /nF	11.779	Number of turns for Loop 3 N_3	10

To verify that the output voltage could keep constant as load varies, we change the load from $12\ \Omega$ to $200\ \Omega$. Figure 6 shows the DC-DC efficiency and output voltage respectively while load varies.

**Figure 6.** Output voltage and efficiency respectively versus load resistance for the 3-coil system.

From Figure 6, the maximum voltage is 63.85 V, the minimum voltage is 60.39 V. Obviously, constant voltage output is achieved with only 5.5% output voltage changing rate as load varies from $12\ \Omega$ to $200\ \Omega$. It would show later in Figure 7 that when load varies from $12\ \Omega$ to $120\ \Omega$, the voltage changing rate decreases to 5.1%.

Figure 7 shows the waveforms of voltage V_{in} output from the inverter, current I_{in} output from the rectifier, voltage V_B on the load, current I_B going through the load. Figure 7a shows these waveforms corresponding to $12\ \Omega$, with $V_B = 60.39\ \text{V}$ and $I_B = 5.03\ \text{A}$, meaning that the output power is 303.76 W, and the transfer efficiency is 90.58%. Figure 7b shows the waveforms corresponding to $120\ \Omega$, with $V_B = 63.64\ \text{V}$ and $I_B = 0.53\ \text{A}$, meaning that the output power is 33.62 W, and the transfer efficiency is 72.46%. Comparing these two working conditions, we can conclude that the voltage changing rate is 5.1%, almost achieving constant voltage output goal.

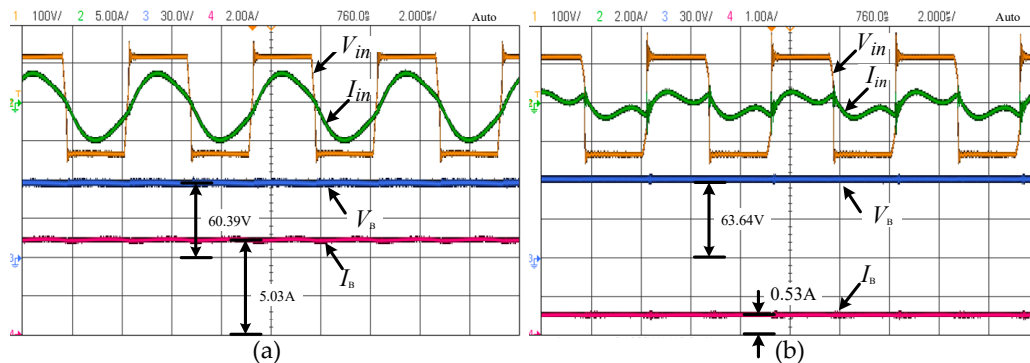
**Figure 7.** Experimental waveforms of V_{in} , I_{in} , V_B , I_B at (a) $R_L = 12\ \Omega$ (b) $R_L = 120\ \Omega$.

Figure 8 shows the waveforms of the voltage V_{in} and the current I_{in} respectively, and the voltage V_{GS} and the voltage V_{DS} between gate and source, drain and source of the MOSFET respectively.

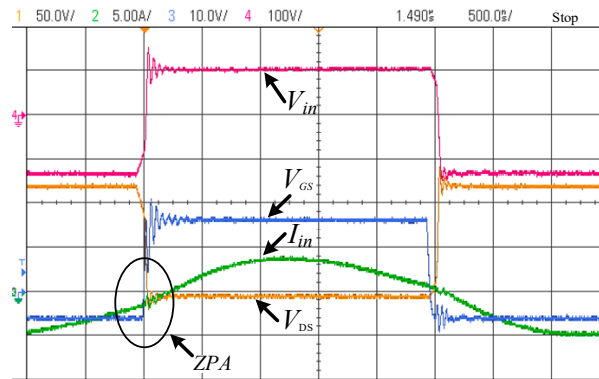


Figure 8. Experimental waves of V_{in} , I_{in} , V_{DS} , V_{GS} .

Based on the waveforms of Figure 8, it's very clear that V_{in} and I_{in} correspond simultaneously to the MOSFET gate driving signal: as the MOSFET turn-on signal V_{GS} goes high, V_{DS} and I_{in} both immediately respond, V_{DS} drops almost to zero as I_{in} starts flowing from drain terminal to source terminal of the MOSFET, proving that the output voltage V_{in} and the output current I_{in} are in the same phase, with no reactive power dissipation.

Figure 9 shows the transient waveforms of V_{in} and I_{in} , V_B and I_B respectively, as switching load from $12\ \Omega$ to $50\ \Omega$ and inversely switching. It's clear that during the switching period, V_B keeps almost constant, and waveforms of I_{in} and V_{in} have no obvious overshoot or undershoot, avoiding spike pulse and achieving stability.

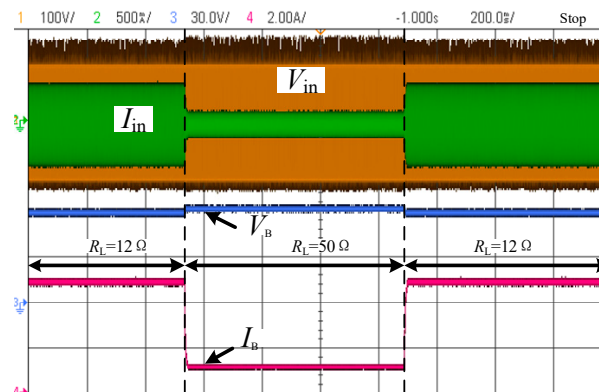


Figure 9. The transient waveforms of V_{in} , I_{in} , V_B , I_B when the load switches between $12\ \Omega$ and $50\ \Omega$.

To prove that the 3-coil system could relieve efficiency falls better than the 2-coil system, we built an S-LCL compensated 2-coil system simulating model with the resonant tank shown in Figure 4. The magnetic simulations are run in ANSOFT Maxwell (Ozen Engineering, Inc., Silicon Valley, Sunnyvale, CA, USA), getting mutual-inductances and self-inductances. MATLAB/Simulink (2014a, Natick, MA, USA) was used to build the system, which could simulate the current and analyze the efficiency.

The coupling mechanism for the 3-coil system in Maxwell simulation is shown in Figure 2b. Coupling mechanism of the transmitter side for the 2-coil system is connecting transmitter coil and relay coil in series. Loop 3 and loop 1 is same centered, and the outer diameter for loop 3 is 300 mm, the gap between loop 1 and loop 3 is 40 mm; loop 1 and loop 2 both have 191.5 mm diameter. These 3 coils each has 10 turns, the winding resistance r_1 , r_2 , r_3 is $0.18\ \Omega$, $0.18\ \Omega$, and $0.29\ \Omega$ respectively.

Taking 10 mm steps, increasing transfer distance from 100 mm to 200 mm, the mutual-inductance between each coil for both systems got with ANSOFT Maxwell are show in Table 2, where subscription 1, 2 and 3 represent transmitter coil, receiver coil and relay coil, respectively; the changing trend is shown in Figure 10.

Table 2. Parameters for coupling mechanism for both systems.

Model	gap/mm	100.00	110.00	120.00	130.00	140.00	150.00	160.00	170.00	180.00	190.00	200.00
3 coil	$L_1/\mu\text{H}$	62.51	62.23	61.94	61.87	61.73	61.64	61.49	61.54	61.54	61.46	61.56
	$L_2/\mu\text{H}$	62.57	62.35	61.96	61.98	61.82	61.61	61.57	61.73	61.65	61.71	61.61
	$L_3/\mu\text{H}$	107.14	106.82	106.20	106.26	105.53	105.54	105.57	105.37	105.25	105.42	105.32
	$M_{12}/\mu\text{H}$	9.93	8.38	7.13	6.09	5.23	4.52	3.92	3.41	2.98	2.61	2.30
	$M_{13}/\mu\text{H}$	23.66	23.20	22.91	22.71	22.51	22.40	22.34	22.27	22.28	22.19	22.16
	$M_{23}/\mu\text{H}$	13.04	11.46	10.09	8.92	7.88	7.00	6.23	5.55	4.96	4.44	3.98
2 coil	$L_1/\mu\text{H}$	216.98	215.45	213.96	213.54	212.29	211.99	211.75	211.46	211.34	211.27	211.19
	$L_2/\mu\text{H}$	62.57	62.35	61.96	61.98	61.82	61.61	61.57	61.73	61.65	61.71	61.61
	$M/\mu\text{H}$	22.97	19.84	17.22	15.00	13.11	11.52	10.16	8.96	7.94	7.05	6.28

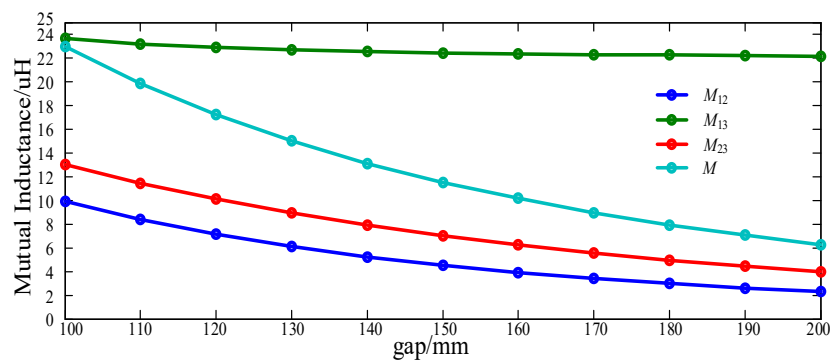


Figure 10. Mutual-inductance Versus Transfer distance.

To verify that the proposed CV model could reduce efficiency fall when transfer distance increases, we simulate the proposed 3-coil system (shown in Figure 1) and the S-LCL compensated 2-coil system (shown in Figure 4) with MATLAB/Simulink. The requirements for a 3-coil system are: setting the load resistance as $12\ \Omega$, keeping the output voltage as 60 V by manually adjusting the input voltage. The requirements for 2-coil system are: setting the load resistance as $12\ \Omega$, keeping the same input voltage as its 3-coil counterpart, adjusting parameter L_{p1} , L_{p2} , and C_{p1} to keep 60 V output voltage. The simulation results are shown in Table 3. Where I_1 , I_2 and I_3 are the current flowing through transmitter coil, receiver coil and relay coil, respectively.

Table 3. Simulating result.

Model	gap/mm	100.00	110.00	120.00	130.00	140.00	150.00	160.00	170.00	180.00	190.00	200.00
3 coil	Pin/w	329.80	325.70	323.10	326.40	327.60	331.90	332.60	336.10	344.40	347.70	356.20
	Pout/w	306.30	302.20	299.20	301.10	300.70	301.90	300.10	299.10	301.30	299.60	300.10
	$\eta/\%$	92.89	92.78	92.62	92.24	91.79	90.96	90.24	88.99	87.50	86.15	84.26
	U_{RL}/V	60.62	60.22	59.92	60.11	60.07	60.19	60.01	59.91	60.13	59.96	60.01
	E/V	117.20	129.50	144.10	161.80	181.00	203.00	226.50	253.00	284.00	315.00	351.00
	I_1/A	3.13	2.80	2.50	2.25	2.03	1.84	1.67	1.53	1.42	1.33	1.27
	I_2/A	5.61	5.58	5.53	5.57	5.56	5.57	5.56	5.55	5.57	5.55	5.56
	I_3/A	4.21	4.43	4.78	5.28	5.87	6.56	7.30	8.16	9.14	10.17	11.34
2 coil	Pin/w	325.00	324.20	325.40	328.40	334.60	345.50	362.30	390.80	435.80	504.50	613.60
	Pout/w	301.00	300.50	300.70	300.70	300.70	300.50	300.10	300.20	299.30	299.30	300.20
	$\eta/\%$	92.61	92.69	92.41	91.57	89.87	86.98	82.81	76.81	68.67	59.33	48.92
	U_{RL}/V	60.10	60.05	60.07	60.07	60.07	60.05	60.01	60.02	59.93	59.93	60.02
	E/V	117.20	129.50	144.10	161.80	181.00	203.00	226.50	253.00	284.00	315.00	351.00
	I_1/A	3.12	2.82	2.55	2.33	2.33	2.01	1.88	1.80	1.76	1.81	1.96
	I_2/A	3.53	4.54	5.86	7.58	9.74	12.47	15.81	20.04	25.41	31.76	39.75

Based on data in Table 3, for the 2-coil system, currents (I_1 , I_2) versus transfer distance are drawn in Figure 11. It's obvious that as transfer distance increases, I_1 decreases firstly, but when the coupling coefficient becomes very weak, loss of system becomes excessive large, resulting I_1 increases. For I_2 , it increases from 3.5 A to 39.7 A, leading to increasing loss and decreasing efficiency.

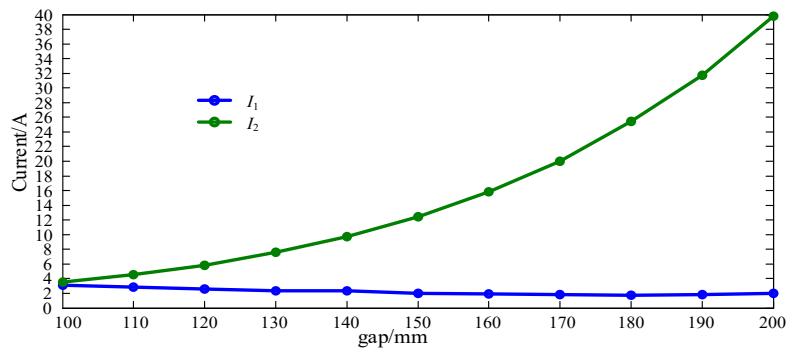


Figure 11. Current Versus Transfer Distance for 2-coil System.

For the 3-coil system, currents (I_1 , I_2 , I_3) versus transfer distance are drawn in Figure 12. It's clear that as transfer distance increases, I_1 decreases continually, I_2 keeps almost constant, and I_3 increases from 4.2 A to 11.3 A, leading to lower efficiency but better than that of 2-coil system.

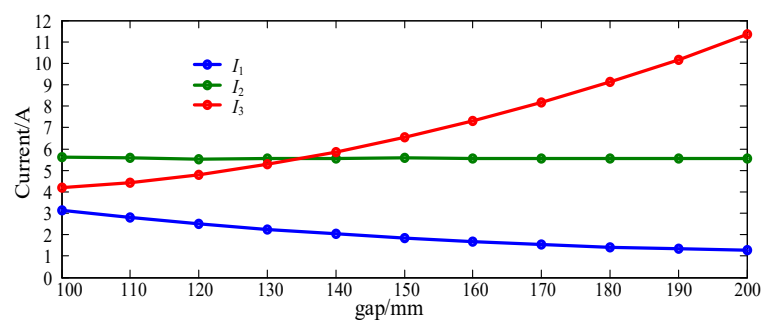


Figure 12. Current Versus Transfer Distance for 3-coil System.

For the two systems, their efficiency trends are shown in Figure 13. It could be seen that as transfer distance increases, the efficiency decreases from 92.61 to 48.9% for the 2-coil system, and it decreases from 92.89 to 84.26% for the 3-coil system. Proving that the proposed model could improve the transfer efficiency as power transfer distance increases.

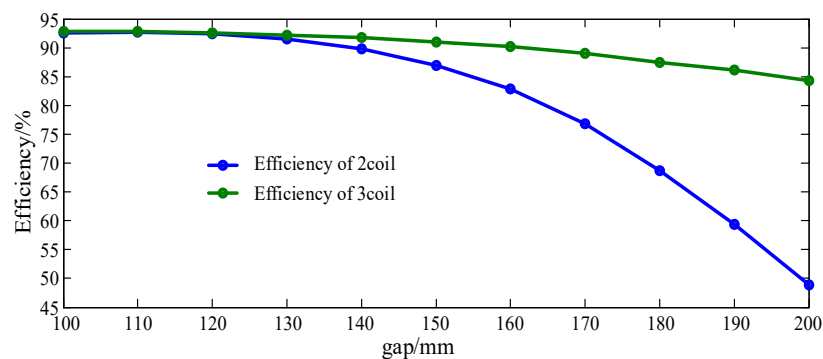


Figure 13. Mutual-inductance Versus Transfer Distance.

4. Conclusions

This essay proposes a SS compensated 3-coil IPT system to achieve CV and ZPA conditions, solving the efficiency decreasing problem in long distance coupling for the traditional 2-coil IPT system. This proposal has no complicated control circuit, and the output voltage only involves the ratio of mutual-inductances between the coils. In the CV verification experiment, the voltage change rate is 5.5% as the load varies from 12 Ω to 200 Ω , with 100 mm transfer distance. In the simulated comparing experiment, as transfer distance increases from 10 cm to 20 cm, transfer efficiency for 2-coil system decreases from 92.61 to 48.9%, for 3-coil system from 92.89 to 84.26%. The experiment results prove that the proposed prototype could achieve CV and that the 3-coil system has a higher efficiency than the 2-coil system when increasing transfer distance. Thus, the proposal is feasible and effective to achieve CV as well as ZPA conditions.

Acknowledgments: This paper was supported by National Key R&D Program of China (2017YFB1201002), the National Natural Science Foundation of China under Grant (No. 51677155), the Sichuan Youth Science & Technology Foundation (No. 2016JQ0033), the Fundamental Research Funds for the Central University (No. 2682017QY01).

Author Contributions: Ruikun Mai and Yang Chen proposed the main idea. Youyuan Zhang designed and performed the experiment. Ruimin Dai wrote the paper. All the authors have read and approved the final manuscript.

Conflicts of Interest: The authors declare no conflict of interest.

References

1. Zhang, X.; Yang, Q.; Chen, H.; Li, Y.; Cai, Y.; Jin, L. Modeling and Design and Experimental Verification of Contactless Power Transmission Systems via Electromagnetic Resonant Coupling. *Proc. CSEE* **2012**, *32*, 153–158. (In Chinese)
2. González-González, J.M.; Triviño-Cabrera, A.; Aguado, J.A. Design and Validation of a Control Algorithm for a SAE J2954-Compliant Wireless Charger to Guarantee the Operational Electrical Constraints. *Energies* **2018**, *11*, 604. [[CrossRef](#)]
3. Liu, Y.; Hu, A.P. Study of Power Flow in an IPT System Based on Poynting Vector Analysis. *Energies* **2018**, *11*, 165. [[CrossRef](#)]
4. Fan, X.; Mo, X.; Zhang, X. Research Status and Application of Wireless Power Transmission Technology. *Proc. CSEE* **2015**, *35*, 2584–2600. (In Chinese)
5. Li, Y.; Mai, R.; Lu, L.; He, Z. Active and Reactive Currents Decomposition based Control of Angle and Magnitude of Current for a Parallel Multi-Inverter IPT System. *IEEE Trans. Power Electron.* **2017**, *32*, 1602–1614. [[CrossRef](#)]
6. Hu, G.; Zhang, J.; Wang, J.; Fang, Z.; Cai, C.; Lin, Z. Combination of Compensations and Multi-Parameter Coil for Efficiency Optimization of Inductive Power Transfer System. *Energies* **2017**, *10*, 2088. [[CrossRef](#)]
7. Lu, F.; Zhang, H.; Mi, C. A Review on the Recent Development of Capacitive Wireless Power Transfer Technology. *Energies* **2017**, *10*, 1752. [[CrossRef](#)]
8. Mai, R.; Li, Y.; He, Z.; Yang, M.; Lu, L.; Liu, Y.; Chen, Y.; Lin, T.; Xu, D. Wireless Power Transfer Technology and Its Research Progress In Rail Transportation. *J. Southwest Jiaotong Univ.* **2016**, *51*, 446–461. (In Chinese)
9. Sallán, J.; Villa, J.L.; Llombart, A.; Sanz, J.F. Optimal Design of ICPT Systems Applied to Electric Vehicle Battery Charge. *IEEE Trans. Ind. Electron.* **2009**, *56*, 2140–2149. [[CrossRef](#)]
10. Mai, R.; Ma, L. Research on Inductive Power Transfer Systems with Dual Pick-up Coils. *Proc. CSEE* **2016**, *36*, 5192–5199. (In Chinese)
11. Fareq, M.; Fitra, M.; Irwanto, M.; Syafruddin, H.S.; Gomesh, N.; Farrah, S.; Rozailan, M. Solar wireless Power Transfer Using Inductive Coupling for Mobile Phone Charger. In Proceedings of the 2014 IEEE 8th International Power Engineering and Optimization Conference (PEOCO2014), Langkawi, Malaysia, 24–25 March 2014; pp. 473–476.
12. Xu, W.; Liang, W.; Peng, J.; Liu, Y.; Wang, Y. Maximizing Charging Satisfaction of Smartphone Users via Wireless Energy Transfer. *IEEE Trans. Mob. Comput.* **2017**, *16*, 990–1004. [[CrossRef](#)]

13. Kang, W.; Alexander, Z.; Jun, H.; Park, Y.; Pack, J. Exposure Assessment for a Wireless Multi-Phone Charger. In Proceedings of the 2014 International Symposium on Electromagnetic Compatibility, Tokyo, Japan, 12–16 May 2014; pp. 198–201.
14. Chung, E.; Lee, J.; Ha, J. System Conditions Monitoring Method for a Wireless Cellular Phone Charger. In Proceedings of the 2014 International Power Electronics and Application Conference and Exposition, Shanghai, China, 5–8 November 2014; pp. 639–643.
15. Li, H.; Li, J.; Wang, K.; Chen, W.; Yang, X. A maximum Efficiency Point Tracking Control Scheme for Wireless Power Transfer Systems Using Magnetic Resonant Coupling. *IEEE Trans. Power Electron.* **2015**, *30*, 3998–4008. [[CrossRef](#)]
16. Mai, R.; Zhang, Y.; Chen, Y.; Kou, Z.; He, Z. Study on IPT Charging System with Hybrid Topology for Configurable Charge Currents. *Proc. CSEE* **2017**. (In Chinese) [[CrossRef](#)]
17. Boys, J.T.; Covic, G.A.; Xu, Y. DC Analysis Technique for Inductive Power Transfer Pick-ups. *IEEE Power Electron. Lett.* **2003**, *1*, 51–53. [[CrossRef](#)]
18. Vu, V.B.; Doan, V.T.; Pham, V.L.; Choi, W. A new method to implement the constant Current-Constant Voltage charge of the Inductive Power Transfer system for Electric Vehicle applications. In Proceedings of the IEEE Transportation Electrification Conference and Expo, Busan, Korea, 1–4 June 2016; pp. 449–453.
19. Wu, H.H.; Gilchrist, A.; Sealy, K.D.; Bronson, D. A High Efficiency 5 kW Inductive Charger for EVs Using Dual Side Control. *IEEE Trans. Ind. Inform.* **2012**, *8*, 585–595. [[CrossRef](#)]
20. Mai, R.; Chen, Y.; Liu, Y. Compensation Capacitor alteration Based IPT Battery Charging Application with Constant Current and Constant Voltage Control. *Proc. CSEE* **2016**, *36*, 5816–5821. (In Chinese)
21. Mai, R.; Chen, Y.; Zhang, Y.; Li, Y.; He, Z. Study on Secondary Compensation Capacitor alteration Based IPT Charging System. *Proc. CSEE* **2017**, *33*, 3263–3269. (In Chinese)
22. Mai, R.; Chen, Y.; Li, Y.; Zhang, Y.; Cao, G.; He, Z. Inductive Power Transfer for Massive Electric Bicycles Charging Based on Hybrid Topology Switching with A Single Inverter. *IEEE Trans. Power Electron.* **2017**, *8*, 5897–5906. [[CrossRef](#)]
23. Kiani, M.; Jow, U.M.; Ghovanloo, M. Design and optimization of a 3-coil inductive link for efficient wireless power transmission. *IEEE Trans. Biomed. Circuits Syst.* **2011**, *5*, 579–591. [[CrossRef](#)] [[PubMed](#)]
24. Tran, D.H.; Vu, V.; Choi, W. Design of a High Efficiency Wireless Power Transfer System with Intermediate Coils for the On-board Chargers of Electric Vehicles. *IEEE Trans. Power Electron.* **2017**, *1*, 175–187. [[CrossRef](#)]
25. Kurs, A.; Karalis, A.; Moffatt, R.; Joannopoulos, J.D.; Fisher, P.; Soljacic, M. Wireless power transfer via strongly coupled magnetic resonances. *Science* **2007**, *317*, 83–86. [[CrossRef](#)] [[PubMed](#)]
26. Beh, T.C.; Kato, M.; Imura, T.; Oh, S.; Hori, Y. Automated Impedance Matching System for Robust Wireless Power Transfer via Magnetic Resonance Coupling. *IEEE Trans. Ind. Electron.* **2013**, *60*, 3689–3698. [[CrossRef](#)]
27. Zhong, W.X.; Zhang, C.; Liu, X.; Hui, S.Y.R. A Methodology for Making a Three-Coil Wireless Power Transfer System More Energy Efficient Than a Two-Coil Counterpart for Extended Transfer Distance. *IEEE Trans. Power Electron.* **2015**, *30*, 933–942. [[CrossRef](#)]
28. Moon, S.; Kim, B.C.; Cho, S.Y.; Ahn, C.H.; Moon, G.W. Analysis and design of a wireless power transfer system with an intermediate coil for high efficiency. *IEEE Trans. Ind. Electron.* **2014**, *61*, 5861–5870. [[CrossRef](#)]
29. Kim, J.W.; Son, H.C.; Kim, K.H.; Park, Y.J. Efficiency analysis of magnetic resonance wireless power transfer with intermediate resonant coil. *IEEE Antennas Wirel. Propag. Lett.* **2011**, *10*, 389–392. [[CrossRef](#)]
30. Zhang, F.; Hackworth, S.A.; Fu, W.; Li, C.; Mao, Z.; Sun, M. Relay effect of wireless power transfer using strongly coupled magnetic resonances. *IEEE Trans. Magn.* **2011**, *47*, 1478–1481. [[CrossRef](#)]
31. Moon, S.; Moon, G.W. Wireless Power Transfer System with an Asymmetric Four-Coil Resonator for Electric Vehicle Battery Chargers. *IEEE Trans. Ind. Electron.* **2016**, *31*, 6844–6854.
32. Ahn, D.J.; Hong, S.C. A study on magnetic field repeater in wireless power transfer. *IEEE Trans. Ind. Electron.* **2013**, *60*, 360–371. [[CrossRef](#)]
33. Kamineni, G.; Covic, A.; Boys, J.T. Analysis of Coplanar Intermediate Coil Structures in Inductive Power Transfer Systems. *IEEE Trans. Power Electron.* **2015**, *30*, 6141–6154. [[CrossRef](#)]

